ACS Catalysis

Research Article

Cite This: ACS Catal. 2019, 9, 10305−10316

pubs.acs.org/acscatalysis

Elucidating Acidic Electro-Oxidation Pathways of Furfural on Platinum

Alex M. Román,[†,‡] Joseph C. Hasse,[†,‡] J. Will Medlin,[†,‡] and Adam Holewinski*[,†,‡]

[†]Department of Chemical and Biological Engineering and [‡]Renewable and Sustainable Energy Institute, University of Colorado Boulder, Boulder, Colorado 80309, United States

Supporting Information

ABSTRACT: Electrocatalysis poses a number of possible advantages for the valorization of biomass-derived feedstocks, most critically its amenability to direct conversion in acidic aqueous media. Furanic biomass derivatives, such as furfural, are substrates with a number of value-added chemical outlets via partial oxidation, most notably furoic acid (FA), a potential precursor to 2,5-furandicarboxylic acid (FDCA). Pairing such partial oxidations with H_2 evolution or other reduction reactions (e.g. CO_2) in an electrochemical cell presents an opportunity to perform electrolysis at lowered voltages, while coproducing products that are more valuable than O_2. Here, we have utilized differential reactor studies with online electrochemical mass spectrometry (OLEMS), as well as in situ infrared spectroscopy attenuated total reflectance-surface-enhanced infrared reflection-absorption spectroscopy (ATR-SEIRAS), to probe the oxidative reaction pathways of furfural on platinum catalysts in acidic electrolyte. We find furfural electro-oxidation selectivity to depend on potential, with the largest shifts corresponding to the transition of Pt to Pt-oxide. Below 1.2 V_{RHE}, FA and 5-hydroxyfuroic acid are the primary products. At higher potential, selectivity shifts predominantly toward 5-hydroxy-furan-2(5*H*)-one (HFN), with the appearance of maleic acid (MA) as well. ATR-SEIRAS and OLEMS indicate that decomposition and overoxidation to CO_2 occurs via decarbonylated or decarboxylated ring intermediates, while MA is less easily activated toward further oxidation once it is formed. Significant oxidative currents are only achieved at potentials where the surface is cleared of CO, which is derived from spontaneous decarbonylation of furfural on the metallic Pt surface. As potential is increased, selectivity to C_4 and C_5 oxygenates over CO_2 is then promoted by a high steady-state surface coverage of organic intermediates that inhibit rapid adsorption and addition of oxygen from the discharge of water. Based on these findings, we propose a reaction pathway and directions for the design of more active and selective electrocatalysts.

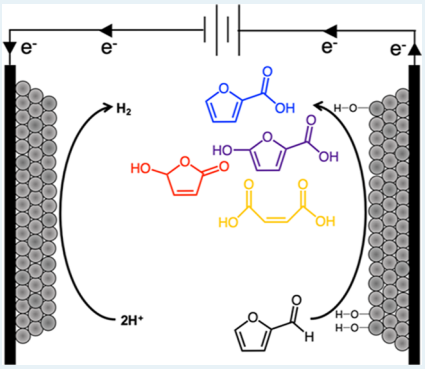

KEYWORDS: *furfural, furoic acid, electrochemical oxidation, platinum, OLEMS, electrocatalysis, differential electrolysis flow cell, biomass conversion*

INTRODUCTION

Electrocatalysis provides an intriguing route for the valorization of biomass-derived intermediates. Electrochemical processes have benefits including the ability to operate at ambient conditions, generation of oxidative or reducing equivalents in situ, and compatibility with the acidic, aqueous feedstocks that result from most conventional biomass-processing techniques.[1−3] It is thus not surprising that a resurgent interest in electrochemical organic synthesis methods has accompanied growth in biomass-derived commodity production and a continual decrease in renewable electricity costs.[4] Furanic derivatives such as furfural and 5-hydroxymethylfurfural (HMF) are substrates of prime interest as they are produced directly from the acid hydrolysis of several biomass feedstocks and represent a synthetic platform for numerous value-added compounds.[5] "Drop-in" biofuels can be produced from both species by reduction chemistries (hydrogenation/hydrodeoxygenation),[6−9] while partial oxidations can yield various fine chemicals. Major chemical targets for furfural include furoic acid (FA)[10,11]—a common preservative, fungicide, and pharmaceutical precursor—and maleic acid (MA),[12−18] of which 25 kton/yr is produced for polymer resins, flavorants, and a variety of niche syntheses by Diels−Alder chemistry.[19] Another product, 5-hydroxy-2(5*H*)-furanone (HFN), shows promise as a feedstock for pharmaceutical, rubber additive, and agrochemical compounds such as γ-butyrolactone.[19,20] HMF is most commonly slated toward production of the monomer 2,5-furandicarboxylic acid (FDCA), but HMF production has yet to surpass the pilot plant scale and relies on the conversion of edible C_6-sugars. In contrast, furfural production already exceeds 300 kton/yr and is largely derived from xylose, a product of the less valuable hemicellulose.[19,21] Furfural can also be used as an FDCA precursor; after initial oxidation of furfural to FA, a subsequent

Received: June 24, 2019
Revised: August 24, 2019
Published: September 25, 2019

DOI: 10.1021/acscatal.9b02656
ACS Catal. 2019, 9, 10305−10316

carboxylation to FDCA can be performed using atmospheric CO_2 in the aqueous-phase. Preliminary technoeconomic analyses have suggested this path to FDCA to be scalable.[22−24]

Present approaches to furan valorization often involve separation from the aqueous phase followed by thermochemical processing, generally at high temperature and pressure.[25] Direct aqueous phase catalytic conversions (both homogeneous and heterogeneous) have also been demonstrated, though these routes still require either strong chemical reagents (e.g. oxidation by H_2O_2, reduction by $NaBH_4$) or elevated temperature (energy intensive with the sensible heat of water) and large O_2 or H_2 pressure.[21,26] Aqueous reforming to light alkanes and H_2 has also been investigated, though with similar harsh conditions.[27,28] Electrochemical routes have been investigated sparingly, but recent efforts in process development suggest economic promise for related electrochemical biomass conversions.[29] Electrocatalytic hydrogenation of furfural to fuels[6−8,30] has received the most attention, followed closely by electro-oxidation routes for HMF to FDCA.[31−38] Very few studies have investigated electro-oxidation of furfural, and, with the exception of one recent study,[39] each instance has involved either nonaqueous or alkaline environments that are less representative of biomass hydrolysis feedstocks.[39−42] Several products of furfural electro-oxidation have been identified, but overall pathways and mechanistic details are far from established. A recent density functional theory study of furfural electro-oxidation on Pt(111) did find several possible paths, with FA being the most energetically favorable product,[43] but changes to the surface structure at high potential keep many mechanistic questions open.

Here, we have utilized differential reactor studies with online mass spectrometry, in situ electrochemical attenuated total reflectance-surface-enhanced infrared reflection-absorption spectroscopy (ATR-SEIRAS), and electroanalytical methods to gain insights into the reaction mechanism of furfural electro-oxidation on carbon-supported Pt in acidic media. Pt provides a useful starting point for assessing features of the reaction as it is corrosion-resistant in acid,[44] active in a number of organic electro-oxidation applications (such as direct-alcohol fuel cells[45,46]), and selective to FA under thermochemical conditions.[47] We find that furfural electro-oxidation occurring between 0.9 and 1.1 V_{RHE} has high selectivity to FA and 5-hydroxyfuroic acid (HFA). At 1.2 V_{RHE} and above, HFN becomes a major product, with an increase in selectivity toward MA as well. To our knowledge, this is the first time that HFN has been identified as an aqueous electrochemical oxidation product of furfural, while HFA has not previously been reported as a product of furfural oxidation, electrochemically or otherwise. Tuning the electrocatalyst toward high FA selectivity could replace current FA production via the Cannizzaro reaction, which requires alkalinization and yields disproportionation products.[2] Finally, we combine studies using IR spectroscopy and online mass spectrometry with stripping voltammetry of various products and proxies for intermediate species to deduce a plausible reaction mechanism, from which we propose directions for the design of more active and selective electrocatalysts.

EXPERIMENTAL METHODS

Materials. All solutions were prepared using ultrapure (UP) deionized water (>18.2 MΩ cm, Millipore). Furfural (99%, Sigma-Aldrich) was purified by vacuum distillation and then stored at −70 °C until needed in experiments. All other reagents and standards were used as delivered: Suprapure perchloric acid (70%, MilliporeSigma), Pt gauze (Alfa Aesar), 2-furoic acid (98%, Sigma-Aldrich), 2(5*H*)-furanone (96%, Sigma-Aldrich), 5-hydroxy-2(5*H*)-furanone (96%, Enamine LLC), MA (99%, Sigma-Aldrich), 40% Pt/C (XC-72 support, Premetek, XRD crystallite size = 4−6 nm), Pt Black (Premetek, XRD crystallite size = 7−10 nm), ethanol (200-Proof, Decon Labs Inc.), 5 and 20% (w/w) Nafion solution in aliphatic alcohols (Sigma-Aldrich), argon (UHP, AirGas), hydrogen (UHP, AirGas), 2-propanol (HPLC Grade, Sigma-Aldrich), plain carbon cloth (AvCarb Material Solutions), D_2O (99.9 at. % D, Cambridge Isotope Laboratories, Inc.), 0.05% w/w DSS in D_2O (99.9 at. % D, Sigma-Aldrich).

Differential Electrolysis Flow Cell. A flow-through electrolysis cell was developed and custom built to assess electrolysis catalysts with minimal impact from secondary products and slow homogeneous chemistries. A schematic of the cell design can be found in Figure S1 of the Supporting Information. The body of the cell was constructed from PEEK with a 3 mm ID flow channel. The reference (RE) and counter (CE) electrodes were isolated from the flowing electrolyte via glass bridge tubes tipped with a 1 mm thick Nafion separator. The bridge tube tips were prepared by depositing 50 μL of a 20% Nafion solution into the tips and allowing to dry overnight at 65 °C. The tubes were then backfilled and allowed to soak in an electrolyte solution for 12 h prior to use. The RE consisted of a Pt wire (Alfa Aesar) bubbled over with H_2 to create a reversible hydrogen electrode (RHE). The CE was a Pt wire mesh (Alfa Aesar) with a geometric surface area of ∼4 cm^2. Both the CE and RE were flame-polished and quenched in UP water immediately prior to use. The working electrode (WE) consisted of a Pt ink deposited on a plain carbon cloth. Both the Pt/C and the Pt Black inks were prepared at a concentration of 1 mg_{Pt}/50 μL for 1 mL of total ink containing 0.8 mL 200-proof ethanol, 0.2 mL UP water, and 10 μL 5% Nafion ionomer solution. Inks were sonicated in ice water for at least 1 h prior to application onto the carbon cloth WE.

Electrochemical characterization was performed with a Gamry Reference 3000 potentiostat. Uncompensated resistance (R_u) was evaluated prior to each experiment and typically fell in the range of 5−15 Ω using electrochemical impedance spectroscopy. All currents are reported with *iR*-correction, and all potentials are reported versus RHE. In a typical experiment, 50 mL of electrolyte was de-aerated by bubbling argon gas at 60 sccm for 20 min prior to being pulled into a clean 10 mL syringe. The syringe was then quickly connected to the flow cell using polytetrafluoroethylene (PTFE) tubing and the electrolyte was flowed through the cell at 0.05 mL/min using a syringe pump. A break-in procedure consisted of cycling the catalyst from 0.3−1.3 V at 20 mV/s for 50 cycles prior to use. The electrochemical surface area (ECSA) was measured during cyclic voltammograms in the range of hydrogen adsorption (0.05−0.4 V at 20 mV/s) on the Pt surface, assuming a stripping charge of 210 μC cm_{Pt}^{-2}.[45] After break-in and ECSA determination, a freshly de-aerated electrolyte containing 100 mM furfural was introduced to the cell (at 0.05 mL/min) under potential control at 0.6 V to flush the reactor for 20 min prior to the experiment. This flow rate resulted in a residence-time of ∼8 s through the catalyst bed. Product yields and electron balances were used to estimate the conversion, which was below 2% in all experiments. Higher flow rates did not change the reaction rate or products, and so mass transport effects were deemed negligible.

DOI: 10.1021/acscatal.9b02656
ACS Catal. 2019, 9, 10305−10316

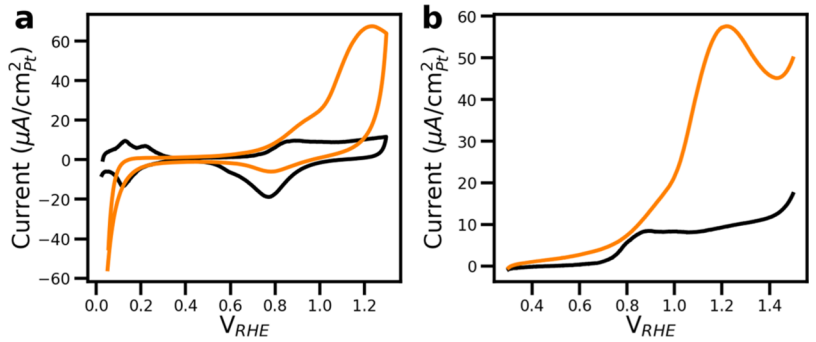

Figure 1. Cyclic (a) and linear-sweep (b) voltammograms for Pt/C in 0.25 M $HClO_4$ without (black) and with 100 mM furfural (orange) present. Scan rate = 20 mV/s.

Chronoamperometry experiments consisted of setting the operating potential for the WE and allowing the reaction to come to steady state over 30 min. The steady-state current was recorded as samples were collected over an additional 30 min into Parafilm-covered 1.5 mL micro-centrifuge tubes. At the end of the experiment, the reactor was purged with a fresh de-aerated electrolyte at 1 mL/min for 20 min. The experimental procedure was then repeated (in blank electrolyte) to assess the minimum current associated with the breakdown of the support material. This background current decays with time and was negligible at all potentials up to 1.0 V and amounted to <10% of the total current at 1.3 V; these currents were background-subtracted from the total current at each potential. Full calculation details for partial currents, selectivity, and Faradaic efficiencies can be found in the Supporting Information. Additional control experiments indicated that product distributions were comparable between Pt/C and Pt black. Each flow reactor experiment was performed in triplicate. The flow cell was cleaned between experiments by sequential sonication in acetone, 2-propanol, and UP water, 30 min each at 50 °C. The cell was then placed into a H_2SO_4/NoChromix cleaning bath overnight to remove residual organic species and then boiled in UP water 5 times prior to use.

Online Electrochemical Mass Spectrometry. The tip of a 1/16″ PEEK tube (ID = 1/32″) was covered by a hydrophobic PTFE pervaporation membrane (50 μm thick, 0.2 μm pore size, Sterlitech), sealed with a water-tight PTFE heat-shrink sleeve and positioned downstream of the WE but upstream of the CE bridge tube. The tubing was directly coupled to the quadrupole vacuum system of a Hiden HPR40 mass spectrometer to acquire data during voltammetry experiments. An electron energy of 70 eV was used for ionization of all species with an emission current of 600 μA. CO_2 (m/z = 44) was detected via a scanning electron multiplier with a detector voltage of 1 kV.

In Situ Infrared Spectroscopy. A Pt nanoparticle film was chemically deposited on the total-reflecting plane of a 25 mm × 25 mm Si hemicylindrical prism (RJ Spectroscopy) via an electroless plating method originally developed by Osawa and others.[48] The base plane of the prism was mechanically polished using progressively finer alumina slurries (5, 0.3, 0.05 μm) as polishing agents. The crystal was then sonicated first in UP water for 20 min and then in a 50:50 mixture of UP water and isopropanol for 20 min. The Si surface was then etched using a 40% NH_4F (Sigma-Aldrich) solution to remove the native oxide layer and terminate the surface with hydrogen.[49] Next, a solution of 0.5 mM $PdCl_2$ with 1% w/w HF was applied to the surface to deposit a Pd adhesion layer.[50] Finally, a 50 °C solution of LECTROLESS Pt100 (Electroplating Engineering of Japan) was added dropwise onto the flat surface of the crystal at 50 °C for 10 min; the solution was then refreshed and left for another 5 min. While this surface was not identical to the supported Pt/C catalysts, the deposition protocol is well established to generate a polycrystalline film with nanoscale roughness.

The SEIRAS measurements were taken in the Kretschmann ATR configuration with an incident angle of 70°.[48] Infrared spectra were recorded using p-polarized light from a Nicolet 6700 FT-IR Spectrometer (Thermo Electron) equipped with a liquid nitrogen-cooled MCT-A detector. The entire apparatus was contained in a N_2-purged Tabletop Optical Module (TOM) box to limit interference from atmospheric CO_2 and water. Spectra were acquired at a resolution of 16 cm^{-1}. A Pt wire in a H_2-saturated electrolyte was isolated via Luggin capillary and served as the reference electrode. A platinum wire mesh served as the CE.

Liquid Chromatography. Reaction products were primarily analyzed by an Advion 2000 HPLC equipped with a UV diode array detector (DAD) as well as an Advion Expression Compact Mass Spectrometer—S Series. The mobile phase consisted of Optima Water (Thermo Scientific) with 0.01% formic acid in isocratic mode at a flow rate of 0.2 mL/min. Undiluted samples collected from the flow cell were filtered through a 0.2 μm hydrophilic PTFE membrane (Millipore) into amber vials. The autosampler temperature was set to 4 °C to minimize degradation of furfural prior to sampling. Aliquots of 100 μL were injected into a 300 mm × 6.5 mm sulfonated polystyrene gel column (Hi-Plex H, Agilent) at 60 °C with eluent diverted for the first 20 min of the method to avoid introduction of the corrosive electrolyte to the ion source. Products were identified using atmospheric pressure chemical ionization alternating positive (3 μA) and negative (25 μA) ionization modes. The source gas (N_2) temperature was set to 300 °C and flowed at 4 L/min. The ionized vapor impinged onto a capillary inlet at 200 °C with a capillary voltage of 120 V. Products were confirmed by injection of a known standard. Products were quantified via UV DAD using the following wavelengths: MA (215 nm), 5-hydroxy-2(5*H*)-furanone (200 nm), and FA (251 nm). External calibration curves were produced from standard solutions made in the working electrolyte.

^{1}H NMR. For species without a commercial standard to characterize with chromatography, additional analysis was carried out by ^{1}H NMR (Bruker AVANCE-III 400 MHz). In a typical experiment, 800 μL of collected electrolyte was

DOI: 10.1021/acscatal.9b02656
ACS Catal. 2019, 9, 10305−10316

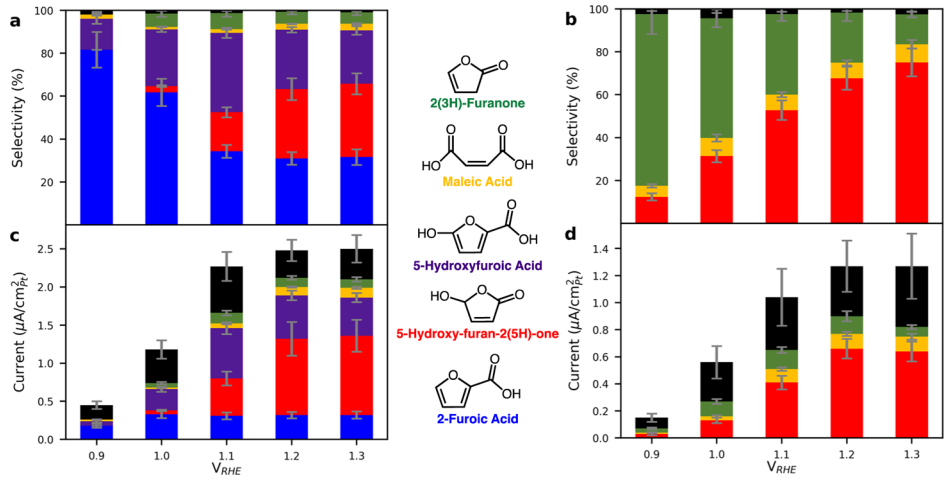

Figure 2. Selectivity and partial currents toward major products of the electro-oxidation of 100 mM furfural (a,c) and 100 mM FA (b,d) on Pt/C in 0.25 M $HClO_4$ at the steady state. FA (blue), 5-hydroxy-2(5*H*)-furanone (red), HFA (purple), MA (yellow), 2(3*H*)-furanone (green), and terminal CO_2 (black) (CO_2 current that is concomitant with C_4 products is allocated to those respectively).

combined with 200 μL of D_2O along with DSS (280 μM) as an internal standard. The sample was then flash-frozen in liquid nitrogen and stored at −70 °C to preserve species until NMR could be performed. A subset of samples was examined using 2D COSY experiments to aid in the structure assignment. Complete details on structure identification are included in the Supporting Information.

RESULTS AND DISCUSSION

Voltammetry of Furfural. The general electrocatalytic features of furfural oxidation on Pt/C were first probed by cyclic voltammetry (CV) in a standard 3-electrode cell with, and without, furfural present in 0.25 M $HClO_4$ electrolyte (Figure 1a). The growth in oxidative current above ∼0.8 V on the anodic scan indicates that furfural oxidation is accessible in this potential region. On the cathodic scan, a reductive process also appears around 0.1 V, consistent with previously reported investigations of furfural electroreduction on Pt.[8] Sweeping voltage to 1.5 V (Figure 1b) confirms that furfural oxidation remains the predominant process until ∼1.45 V where oxygen evolution becomes significant. However, due to evidence of significant carbon support breakdown at potentials higher than 1.3 V, an operating range of 0.9−1.3 V was selected as the potential window for further characterization at the steady state. It may be noted that at the upper end of this window, the furfural oxidation current exhibits an apparent maximum. Pt transitions to an oxide phase in the same region, which alters the activity.[51−53] However, further studies discussed below also indicate that the peak coincides with a high surface coverage of strongly bound organic intermediates, which limit the accessibility of the surface to adsorption of reactive oxygen by discharge of water ($H_2O \rightarrow OH^* + H^+ + e^-$). Initial evidence of surface organic saturation can be seen in rotating disc electrode (RDE) studies with furfural (Figure S2), which reveal that increasing furfural concentration over a wide range (5−100 mM) minimally impacts the voltammogram, with a slight inhibitory effect at a higher concentration.

Steady-State Electro-Oxidation Studies. The product distribution of furfural oxidation was determined using a novel differential electrolysis flow reactor with a Pt/C packed bed electrode (Figure S1). The partial current and selectivity to each major product is reported as a function of potential over the range 0.9−1.3 V in Figure 2. Faradaic efficiencies corresponding to the reaction selectivity can be found in Figure S3. While FA, 5-hydroxy-2(5*H*)-furanone (HFN), MA, and 2(3*H*)-furanone (3FN) have been previously reported in studies of homogeneous and heterogeneous furfural oxidation, HFA has been distinguished as a product for the first time.[15,34] HFA standards were not commercially available, but a combination of ^{1}H NMR (including 2D COSY) and liquid chromatography−mass spectrometry analysis strongly suggest this species (complete details can be found in the Supporting Information).[54] Several trace species, in particular, β-formylpropionic acid, formic acid, and 2(5*H*)-furanone, were also detected in preliminary experiments, but later found to form by slow homogeneous auto-oxidation[55] and isomerization of furfural and 3FN, respectively. Homogeneous chemistry on time scales longer than the reactor residence time (∼5 min) was thus mitigated by flash freezing all samples at −70 °C until analysis.

Figure 2a shows that selectivity of the reaction shifts from primarily $2e^-$ and $4e^-$ oxidation products (FA and HFA, respectively) at 0.9−1.0 V to deeper oxidation products at more elevated potentials. A rather abrupt shift toward the $6e^-$ and $8e^-$ products (HFN and MA) coincides with the well-known transition of the Pt surface to an oxide. In addition to the C_4 and C_5 products, there is an evident pathway toward total oxidation to CO_2. This is consistent with past observations of total electrochemical oxidation for species similar to furfural—namely benzaldehyde[56] and furan[57]—on Pt electrodes under similar conditions. Thus, the CO_2 shown in the product distributions specifically refers to CO_2 generated from the total oxidation route; in contrast, CO_2 generated concomitantly with C_4 products is accounted within the respective C_4 yields. No other C_1, C_2, or C_3 species were detected in the liquid or gas phases, and there was no evidence (spectroscopic or physical) of high molecular weight products such as from oxidative coupling or polymerization, sometimes reported in nonaqueous conditions or with promoters present.[58,59]

It may be noted that the current and product yields plateau at the highest potentials, consistent with the peak behavior observed in Figure 1. Product distributions were confirmed to be constant with increasing electrolyte flow rate and thus not

DOI: 10.1021/acscatal.9b02656
ACS Catal. 2019, 9, 10305−10316

mass transfer limited. The plateau in rate and selectivity is consistent with either (i) transition to limitation by a chemical step (e.g. nonelectrochemical addition of OH* to activated organics) in the limit of high coverage (no changing electrochemical pre-equilibria) or (ii) a stronger potential dependence for adsorption of certain organic surface species than for water discharge onto the Pt oxide surface causing an approach to saturation with organics (blocking oxygen species adsorption).[60,61] The latter is more consistent with the downturn in current at higher potential seen in the linear sweep voltammetry (Figure 1b), and because the reaction is also found to be zero-order with respect to furfural, the surface coverage of organics is expected to be nearly saturated. This is in contrast to the electro-oxidation behavior of less reactive molecules such as aliphatic alcohols, which do not adsorb strongly to Pt oxides and show a peak rate for the opposite reason—water discharge outcompeting the organic adsorption.[62] Features similar to furfural oxidation are found when subsequently oxidizing FA as a starting material.

To assess whether each product is accessible through FA as an intermediate, we repeated the flow reaction experiments with FA as the feed (Figure 2b,d; Faradaic efficiencies in Figure S3). Unlike furfural, FA does not yield HFA, suggesting that this product is produced via an intermediate not accessible from FA. In contrast, at high overpotentials, the production of 3FN, HFN, and MA follows a trend similar to furfural oxidation, indicating that the pathway to C_4 products can proceed through FA. These observations suggest that the decarboxylation of FA is more favorable than the abstraction of H at the 5-position under these conditions. Scheme 1 summarizes an overall proposed pathway linking all major organic furfural electro-oxidation products by sequential oxidations. Known isomerizations are also indicated where they could provide a mechanistic link between the detected products. Further elementary step details are examined in the remainder of this work.

ATR-SEIRAS Studies. Surface species present during furfural oxidation were probed using in situ ATR-SEIRAS on a polycrystalline Pt thin film electrode (Figure S13). The Pt film exhibits nanoscale roughness and is expected to be sufficiently representative of catalyst particle surfaces to illustrate major features of the reaction.[48] Spectra for furfural are shown as a function of potential during a slow CV (5 mV/s) in Figure 3a. The presence of solution-phase furfural is highlighted by an aldehyde carbonyl stretch split between 1672 and 1641 cm^{-1}, consistent with a standard taken without the Pt film present (Figure S14). The beginning of the scan is shown at the bottom of the figure, where the potential of 0.3 V corresponds to the lower end of the double-layer regime of Pt (i.e. negligible coverage of water-derived adsorbates such as H* or OH*). In this region, there is direct evidence that furfural undergoes decarbonylation, indicated by the presence of both linearly bound CO (2075−2025 cm^{-1}, CO_L^*) and multiply bound CO (1815−1825 cm^{-1}, CO_B^*).[63] Previous studies of gas-phase furfural on Pt have indicated that decarbonylation is thermally accessible below room temperature.[64−66] This yields CO, an adsorbed furyl fragment (which may further decompose on Pt[66]), and adsorbed H, which can react with the furyl to make furan, but will be more favored to discharge as $H^+ + e^-$ under oxidative electrochemical conditions. As the potential is increased toward 1.0 V (moving upward in the figure), the CO can be seen to exhibit a strong Stark effect, and it is eventually stripped as CO_2.[50] The CO only reappears when the Pt film is re-reduced on the return scan, at ∼0.7 V.

Aside from solution-phase furfural, the carbonyl region of the spectra exhibits less distinctive signatures; however, a few potential-dependent features can be seen to correlate with the production of oxidized products. Mostly notably, an absorbance at 1711 cm^{-1} emerges at ∼1.2 V in the positive scan and is identified to be FA based on standards. The peak is then persistent on the reverse sweep down to ∼0.8 V before diminishing back to baseline. When compared to product yields, this asymmetry with respect to potential is perhaps surprising but might be understood in terms of the oxide transition of Pt, which exhibits hysteresis during cycling. Previous electrochemical IR studies of similar aromatic carboxylic acids (e.g. benzoic acid, isophthalic acid, etc.) found that deprotonation occurs with increasing potential.[67] This leads to the adoption of a bonding conformation to Pt via the carboxylate oxygens, shifting the carboxylate band below the Si ATR crystal cutoff.[68] We hypothesize that as FA is formed from furfural it builds up mainly as furoate, but that this binding configuration is not favorable on the Pt oxide and molecularly adsorbed or solution-phase FA can be seen on this surface.

To better understand the role of FA as an intermediate, it was also subjected to spectroscopic investigation (Figure 3b). At the starting potential of 0.3 V, a strong peak at 1711 cm^{-1} and a less-prominent peak at 1588 cm^{-1} are assigned to solution-phase FA, matching standards. Interestingly, a small CO peak emerges at low potential and follows a trend similar to that of furfural. The presence of CO derived from FA indicates that CO is not solely generated by the decarbonylation of furfural, but rather that it is possible for adsorbed furyl intermediates (derived from decarboxylation in the case of FA) to undergo decomposition of the ring to CO and $C_xH_y(O)$ fragments, eventually yielding CO_2. CO could also in principle be derived from the decomposition of the carboxylate group; both sources are plausible based on online electrochemical mass spectrometry (OLEMS) discussed below. The primary FA peak (1711 cm^{-1}) drops in magnitude starting around 0.6 V on the forward sweep and re-emerges to its original intensity only after the Pt surface is sufficiently

Scheme 1. Proposed Oxidation Routes Linking Major Products in the Electro-Oxidation of Furfural

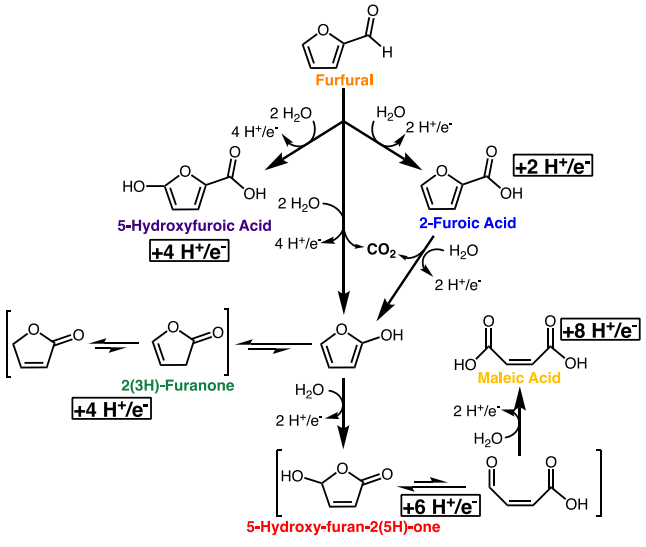

DOI: 10.1021/acscatal.9b02656
ACS Catal. 2019, 9, 10305−10316

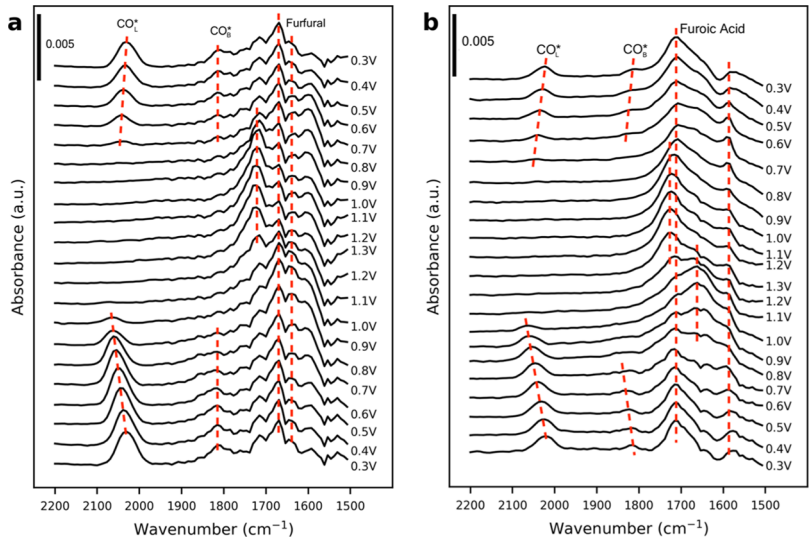

Figure 3. ATR-SEIRAS difference spectra for the electro-oxidation of (a) 100 mM furfural and (b) 100 mM FA in 0.25 M $HClO_4$ on a Pt film. Spectra are referenced to background scans taken at each potential prior to the introduction of the organic. Scan rate = 5 mV/s.

oxidized at ∼1.2 V, consistent with the trend seen for FA in the furfural spectra. Two other features are more clearly resolved than when starting with furfural: (i) a potential dependent shoulder at 1730 cm^{-1} appearing near 1.2 V, suggesting a product coinciding with the onset of Pt oxide and (ii) a more pronounced peak at ∼1660−1630 cm^{-1}, which is evident above 0.8 V but would have overlapped furfural itself. We found that the HFN molecule standard absorbance was a fair bit higher (1767 cm^{-1}), but a standard of 2(5*H*)-furanone shows broad absorbance features across the aforementioned windows. Considering the primary product yields of 3FN and HFN, we assign the peaks nonspecifically to surface-bound furanone species. Related mechanistic possibilities are further investigated below with OLEMS.

Voltammetric Stripping with CO_2-OLEMS. In order to investigate decomposition and the possible interplay between thermally and electrochemically driven pathways, we performed voltammetric stripping experiments with simultaneous OLEMS[69] on furfural (Figure 4) and a number of its partially oxidized products (Figure 5). Each organic species was dosed (after cleaning with voltammetric cycling in blank electrolyte) to the reactor for a fixed-potential adsorption period at 0.3 V. Adsorption was followed by flushing again in organic-free electrolyte with >5 reactor volumes (>15 mL) and finally oxidative stripping at 5 mV/s. Similar to temperature-programmed desorption studies, product selectivities cannot directly be compared to steady-state distributions, but trends in the relative yield of CO_2 to other products provide insight into the relative stability and the surface chemistry of each adsorbed species.

In furfural stripping experiments, onset of oxidation occurs just past ∼0.6 V. An initial peak in CO_2 production is seen at ∼0.75 V, with a secondary peak at ∼1.1 V. Direct stripping of CO and furan under identical conditions (each in a separate experiment) is overlaid in Figure 4. The first peak from furfural (both Faradaic and on MS) appears to align with that of CO stripping (∼0.7 V peak), albeit shifted to slightly higher potentials. The positive shift is likely due to a lesser availability of free sites for water to discharge OH groups onto the surface in the presence of organic furyl-related fragments that remain adsorbed. The primary contribution to the furfural peak is thus

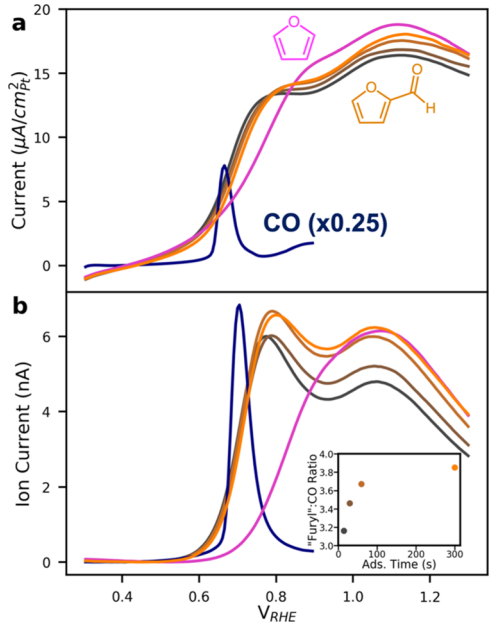

Figure 4. Voltammetric stripping (a) paired with CO_2-OLEMS (b) for furfural (100 mM, 15−300 s adsorption times: black to orange), CO (saturated, navy, ×0.25), and furan (saturated, magenta) after 300 s adsorption periods at 0.3 V_{RHE} on Pt black in 0.25 M $HClO_4$. Inset of (b): ratio of fitted integral "furyl" to CO MS peaks at increasing adsorption times. Scan rate = 5 mV/s and flow rate = 1 mL/min.

assigned to oxidation of CO derived from decarbonylation. As the stripping continues to higher potentials, the CO_2 signal from furfural dips while the Faradaic oxidation current simultaneously increases due to production of organic oxygenates. Comparison between the stripping of furfural and furan shows that the second CO_2-OLEMS feature of furfural (peaking at 1.1 V) aligns well with furan. The Faradaic current associated with the furan stripping is also in agreement but shows a shoulder at ∼0.9 V, preceding CO_2 evolution, and is better illustrated in Figure 5. This indicates that C_4 oxygenate formation is accessible below 1.0 V, while the subsequent large CO_2 signature indicates that there is a further (direct or indirect) pathway at higher potential toward deep

DOI: 10.1021/acscatal.9b02656
ACS Catal. 2019, 9, 10305−10316

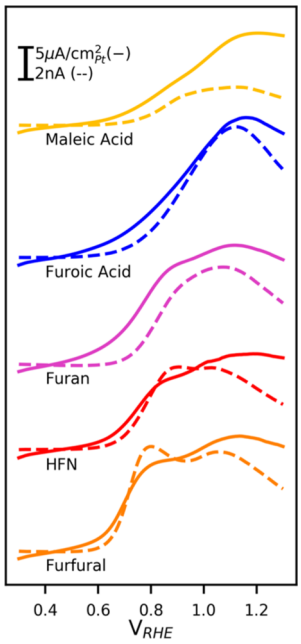

Figure 5. Voltammetric stripping (—) paired with CO_2-OLEMS (--) for furfural (100 mM, orange), HFN (5 mM, red), furan (saturated, magenta), FA (100 mM, blue), and MA (100 mM, yellow) after 300 s adsorption periods at 0.3 V_{RHE} on Pt black in 0.25 M $HClO_4$. Scan rate = 5 mV/s and flow rate = 1 mL/min.

oxidation yielding CO_2 from ring-derived carbon. We thus propose that the rates of oxygenate synthesis and ring decomposition from furan are comparable to those from furfural and that furan is an reasonable proxy for the behavior of furfural after decarbonylation, as well as for FA after decarboxylation. Proposed activation routes for furfural on metallic Pt, based on both ATR and the voltammetric stripping observations, are summarized in Scheme 2.

Scheme 2. Proposed Oxidative Routes toward CO_2 Following the Dissociative Adsorption of Furfural on Pt at Low Potential (0.3 V)

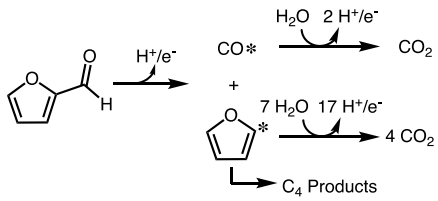

As furfural deposition time is increased, the CO_2 MS signal associated with the stripping of the CO component rises relatively little, while the furyl oxidation component steadily increases. To examine this correlation, the integration of each contribution was approximated via deconvolution into fitted peaks (Figure S15). Ratios of the integrations are compared in the inset of Figure 4b. As the adsorption time is increased, the ratio of CO_2 assigned to furyl oxidation versus CO oxidation asymptotically approaches the theoretical maximum of 4. Higher ratios at longer adsorption times indicate that the proposed surface-furyl decomposes into a species (or multiple fragment species) that is more selectively oxidized to CO_2 (at > 1.0 V) than the furyl precursor. Additionally, the fact that the oxidation of the fragment(s) does not shift to lower potentials or yield smaller currents with longer hold times indicates that the species are strongly bound and do not undergo partial oxidation in the low potential regime. Considering the lack of small organic products in the steady-state experiments, the observed stripping behavior supports a hypothesis that if a pathway removes a carbon from the primary furan ring, the complimentary C_3 or smaller intermediates will preferentially continue toward complete oxidation to CO_2, a $20e^-$ path in total. The initial decomposition steps appear to be thermally accessible on metallic Pt at low potentials but may also proceed on the oxide at higher potentials (chemically or electrochemically).

Stripping experiments were next repeated using products of furfural electro-oxidation: FA, HFN, and MA. The OLEMS stripping voltammograms for each of these species (300 s adsorption periods) are compared to furfural and furan in Figure 5, and data from a modified program used to assess initial coverages and CO_2 selectivity are shown in Figure 6. Complete time-dependent adsorption series for each compound can be found in Figures S16–S19. Based on Faradaic currents alone, the onset of furfural stripping is at the lowest potential (~0.6 V), followed by furan, HFN, FA, and MA stripping, respectively. In contrast to furfural and furan, FA shows greater resilience toward activation processes and has only a single (resolvable) oxidation feature. The current and CO_2 production from FA are relatively insensitive to adsorption time (see Figure S16 in the Supporting Information), indicating that FA adsorption is rapid and that the majority does not decarboxylate by thermal driving force,

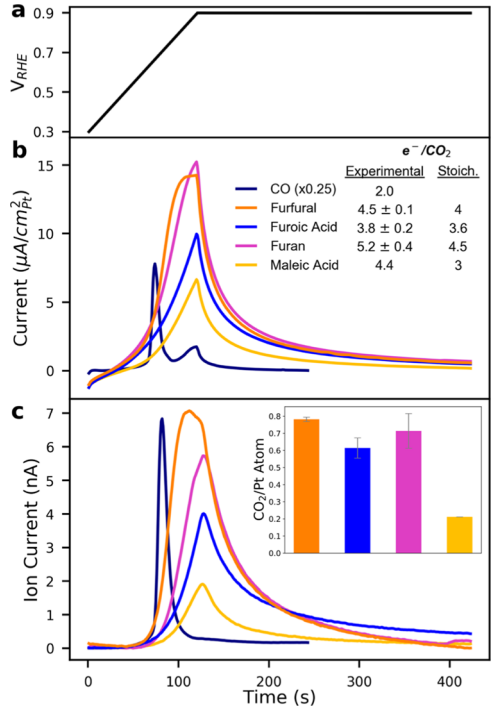

Figure 6. Voltammetric stripping with a 5 mV/s ramp and hold program (a), with Faradaic responses (b) paired with CO_2-OLEMS (c) after 5 min adsorption periods of CO (saturated), 100 mM furfural, 100 mM FA, furan (saturated), and 100 mM MA in 0.25 M $HClO_4$ on Pt Black. Flowrate = 1 mL/min. Insets: number of electrons passed per CO_2 molecule formed for each adsorbate (b) and comparison of relative CO_2 produced per Pt surface atom (c) determined via calibration with CO stripping and CO_2-OLEMS.

DOI: 10.1021/acscatal.9b02656
ACS Catal. 2019, 9, 10305−10316

Scheme 3. Proposed Reaction Mechanism for the Electro-Oxidation of Furfural in Acidic Environment on Pt

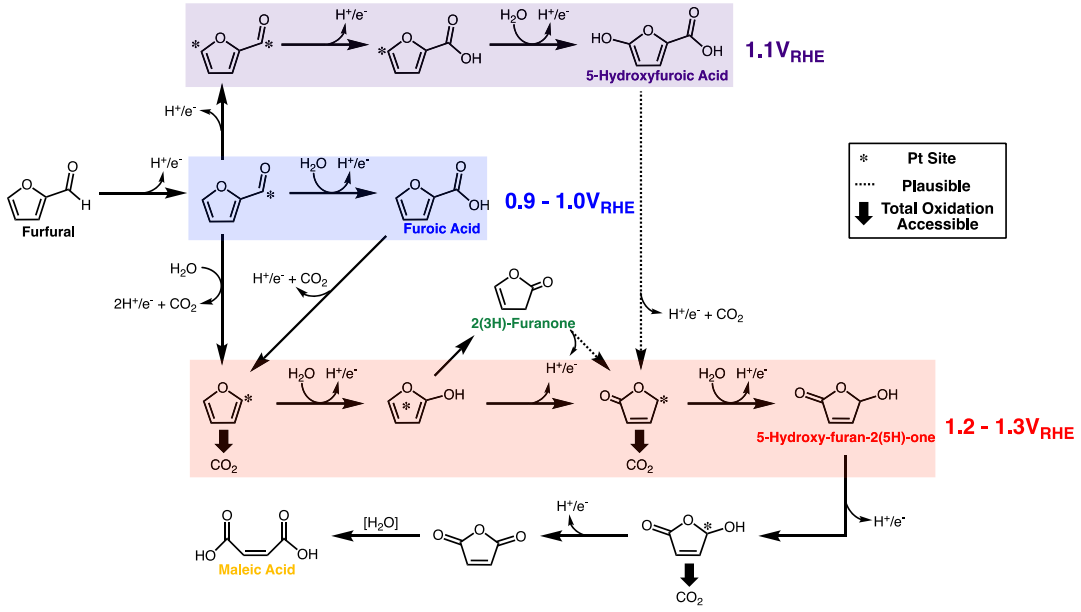

lest it form the more reactive furyl species. Upon onset of oxidation, however, the current and CO_2 signals rise sharply, and the total yield of CO_2 is comparable to that from furfural. Because FA yielded a significant portion of C_4 ring products under steady-state, it is inferred that activation is by decarboxylation; the rapid rise of the total oxidation path after stripping onset for FA is then also consistent with the complementary fragment of decarboxylation being the less stable surface furyl.

HFN stripping shows characteristics more similar to furfural, including an apparent CO feature. It is noteworthy that HFN produces CO_2 earlier than furan, despite having later onset and smaller currents in the Faradaic signal. This is likely due to HFN's equilibrium with the ring-opened isomer β-formylacrylic acid (see Scheme 1), which would facilitate decarbonylation on the Pt surface. Remaining fragments from the ring-opened HFN would then be subjected to further oxidation at higher potentials. Lastly, MA shows the most resilience to oxidation, with a very late onset and low CO_2 yield. We thus note that despite being the most deeply oxidized organic product, MA is not highly susceptible to over-oxidation. The undesirable CO_2 formation routes are accessed from earlier intermediates, indicating that selectivity is critically determined from the stage of surface furyls.

While the product distribution during stripping cannot be directly measured, the yield of electrons per CO_2 molecule (e^-/CO_2) can be interpreted in terms of the balance between paths to CO_2 and oxygenates. To integrate signals without baseline interference from breakdown of carbon components during continuous voltage ramp, stripping experiments were repeated with a potentiostatic hold at 0.9 V after 300 s of adsorption time and purging of the organic. Faradaic and MS signals were calibrated with CO stripping (full calculation details in the Supporting Information), which gives 2 e^-/CO_2 and does not yield other products. Results are summarized in Figure 6, with insets showing both the e^-/CO_2 ratio and normalized integral CO_2 signals. In the modified stripping program, furfural yields 4.5e^-/CO_2 compared to 4e^-/CO_2 for complete stoichiometric oxidation. In comparison, the steady-state oxidation yields in Figure 2a correspond to between 7.8 and 8.9e^-/CO_2 (summarized in Figure S3c). Because steady-state turnover rates (estimated to be 0.001−0.003 s^{-1} for 0.9−1.3 V) represent a surface residence time on the same order of magnitude as the 300 s adsorption period for stripping, the high selectivity to oxygenates at steady state cannot solely be influenced by the rate of surface-mediated decomposition; the surface availability of electrogenerated, reactive oxygen also plays a major role. In the stripping experiments, each product desorption frees up sites that can only be repopulated by reactive oxygen. At steady state, these sites can be blocked by new organic adsorbates that effectively regulate the rate at which oxygen can co-adsorb. While the exact adsorption geometries and ensemble requirements will require further study, each furanic compound in Figure 6 does generate a similar quantity of CO_2 to the adsorbed CO layer. It may thus be inferred that these species tend to approach complete coverage.

The e^-/CO_2 yield from FA is less informative than for furfural because 3FN and HFN are 2e^- and 4e^- decarboxylation paths, while total oxidation gives 3.6e^-/CO_2. However, the total integrated CO_2 production (inset of Figure 6c) nearly matches that of CO, meaning the stripping again mainly yields CO_2, despite its very late onset. Based on earlier evidence that FA is mainly molecularly adsorbed, this shows that, once formed by decarboxylation, surface furyl species undergo total oxidation more readily at high overpotential—i.e., the conditions needed for activation coincide with very high oxygen coverage on the Pt surface. In contrast, furan activation (presumed to be representative of the furyl) occurs at lower potentials, and thus the oxidative stripping gives a much higher e^-/CO_2 yield consistent with more C_4 oxygenate products from this reactant. Taken together, the behavior of FA and furan again suggests that the availability of reactive oxygen species—whether adsorbing on metallic Pt or on top of the Pt oxide phase—strongly influences selectivity. Finally, MA again produces the least CO_2 and has a comparatively high electron yield. A partial oxidation route is thus apparently accessible, although based on the very low total currents and trace steady-

DOI: 10.1021/acscatal.9b02656
ACS Catal. 2019, 9, 10305−10316

state yields, we suggest that this route is negligible when working at higher steady-state surface coverages of intermediates. In summary, the stripping experiments most notably show (i) that CO poisoning may impede a selective path to C_4 species at low potentials, as there is a clear window for furan to partially oxidize without forming CO_2 and (ii) that there is a probable parallel split between total oxidation paths and the pathway terminating with MA.

Proposed Pathways. While thermal furfural oxidation has been studied extensively, oxidation in the electrochemical environment shows both a number of similarities and a number of unique features in comparison to other environments. These can in part be attributed to the transition from metallic Pt to Pt oxide with increasing potential,[45,70] though even in the metallic state some key differences are apparent. The formation of FA is consistent with oxidation studies in other aqueous media (both with peroxide and electrochemically in base),[40] as well as recent computational studies.[43] The electrochemical path diverges from prior studies more markedly with the appearance of HFA. Scheme 3 proposes a more complete reaction mechanism for the oxygenate formation.

To summarize, furfural is initially dehydrogenated at the aldehyde with $H^+ + e^-$ discharge. It then either combines with an OH* to form FA on the Pt surface[71] or an H-abstraction occurs at the 5-position of the ring (which may also occur before the aldehyde dehydrogenation), ultimately leading to HFA. Although a few studies have identified a 5-hydroxyfurfural intermediate to suggest initial abstraction of the 5*H*,[34] we order the sequence to be consistent with a lack of evidence for this product in the electrochemical environment. The 5*H* abstraction could also possibly be aided by equilibrium with the hydrate (gem diol) form of furfural; we again restrict yet-to-be-determined alternatives to focus on the main features. While the ATR-SEIRAS experiments also indicate the possible activation of furfural by initial decarbonylation (commonly cited as an initial step in the heterogeneous reactions of furfural on Pt and Pd surfaces[63]), this path only appears prevalent at low potentials (<0.9 V) where FA is not formed and product yields are in general negligible. We thus propose that the accumulation of CO* serves to block available sites for a kinetically preferred dehydrogenation pathway, preventing steady-state oxidation at lower potentials. Once electro-oxidation of CO* is possible, the surface remains accessible and follows the faster routes toward FA and HFA. Concomitant with the acceleration of electrochemical steps is the increasing degree of oxidation of the Pt surface, which likely also contributes to a poorer ability to perform thermal C−C cleavage steps. Cleavage products only reemerge at the largest driving potentials, suggesting an electron-driven bond cleavage event distinct from decarbonylation yields the majority of C_4 products.

Continuing along Scheme 3, either absorbed furfural or FA can undergo a decarbonylation or decarboxylation step to form an adsorbed furyl species. The behavior of FA in stripping voltammetry (late onset but high CO_2 yield) suggests that the unselective oxidation of the resulting furyl to CO_2 is electrocatalytically driven. The higher proportion of C_4 products observed in steady-state oxidation of FA (compared to stripping) then implies that the coverage of intermediates plays a crucial role in steering selectivity to partial oxidation over total oxidation by limiting the rate at which oxygen can adsorb and add to the reactive species. The C_4 product distribution at steady state also suggests that the furyl that does not act as a gateway to total oxidation and likely passes through 2-furanol. While 2-furanol was never directly observed as a product, the introduction of a commercial standard to the electrolyte environment confirms that 2-furanol readily isomerizes to 3FN [and eventually 2(5*H*)-furanone][72] upon desorption. Considering the inverse relationship between 3FN yield and HFN yield (clearest in Figure 2b,d), it is most likely that 2-furanol is dehydrogenated and then undergoes a subsequent re-arrangement to a surface-bound furanone. This furanone can then be oxidized first to HFN and finally to MA via hydration of the anhydride. Alternative plausible pathways could involve decarboxylation of HFA to bypass the furyl intermediate on the way to HFN and/or 3FN oxidation to HFN. These could not be directly confirmed due to the unavailability of commercial HFA and instability of 3FN toward isomerization to 5FN; however, a proxy experiment with 5FN did yield HFN as a major product. We have thus linked the additional plausible pathways with dotted arrows. Based on the relative stability of both FA and MA, we posit that the unselective degradative CO_2 pathways emanate from adsorbed furyls and furanones.

A major category of alternate furfural oxidation pathways have been suggested to proceed through either 2-formyloxyfuran[73] or 2-oxoglutaconaldehyde,[15,74,75] followed by Baeyer−Villiger oxidation to HFN and formic acid. However, the Baeyer−Villiger rearrangement is only mechanistically achievable with peroxy-intermediates that are unlikely to form in the absence of O_2 or H_2O_2.[76]

CONCLUSIONS

Together, our findings suggest that the selectivity and activity of electrodes used in furfural oxidations can be optimized toward FA production by restricting the furanring from coordinating to the Pt electrode surface and thus preventing decarbonylation/decarboxylation (and the associated total oxidation of the furyl) or 5*H* abstraction leading to HFA. Modifiers that induce an ensemble effect, such as Bi or Pb (which irreversibly adsorb to Pt under electro-oxidation conditions[77,78]) or self-assembled monolayers such as thiolates[79] could sterically hinder furfural[80] and promote higher selectivity toward FA. With sufficiently high selectivity, FA generated through this process could become a feedstock for carboxylation to FDCA with no separation and minimal pretreatment.[23,81] Alternatively, selectivity toward MA and HFN could be targeted through the incorporation of oxophillic metals (e.g. Ru) onto the Pt surface, thereby increasing the surface concentration of reactive OH* species.[82] This type of "bifunctional" Pt alloy or composite is well known to facilitate CO oxidation at milder potentials[83] and could free the metallic Pt surface in a manner that could give C_4 products (by the decarbonylation route) at steady state.

In conclusion, we have observed that the electro-oxidation of furfural on the metallic Pt surface proceeds primarily by the formation of FA, with a significant parallel pathway to HFA production. There is a minor pathway involving initial decarbonylation of furfural, though this is only directly evident at potentials where steady-state oxidation does not occur. Upon transition to complete surface oxidation, the Pt oxide electrode shows an abrupt increase in the rate of C_4 production. Under these conditions, FA (and possibly HFA) is first decarboxylated to yield HFN, eventually resulting in MA. Selectivity toward these products over total oxidation to

DOI: 10.1021/acscatal.9b02656
ACS Catal. 2019, 9, 10305−10316

CO_2 appears to be promoted by a high steady-state coverage of organic species that lower the accessibility of the surface to adsorption of oxygen by water discharge. There remains significant opportunity to enhance the current understanding of this reaction through identification of product distributions on modified electrode materials and additional study of the oxidation behaviors of each intermediate or product found in this work.

■ ASSOCIATED CONTENT

Supporting Information

The Supporting Information is available free of charge on the ACS Publications website at DOI: 10.1021/acscatal.9b02656.

Details on the design of the differential packed bed flow reactor, RDE experiments, sample calculations of selectivity/partial current/Faradaic efficiency, analytical chemistry results (HPLC, LCMS, and NMR), ATR-IR standard spectra, and auxiliary stripping experiments (PDF)

■ AUTHOR INFORMATION

Corresponding Author

*E-mail: adam.holewinski@colorado.edu.

ORCID

Alex M. Román: 0000-0003-0221-4355

J. Will Medlin: 0000-0003-2404-2443

Adam Holewinski: 0000-0001-8307-5881

Notes

The authors declare no competing financial interest.

■ ACKNOWLEDGMENTS

A.M.R. acknowledges support from the NSF Graduate Research Fellowship (#1144083). The authors acknowledge support from the National Science Foundation (CHE 1665176). In addition, the authors would like to thank Dr. Jason Widegren at the National Institute of Standards and Technology (NIST) for assistance running ^{1}H NMR experiments, as well as Adam Baz, Jess Dudoff, Alex Delluva, Taylor Spivey, Grey Garrett, and Dr. Zachary Barton for assistance running experiments.

■ REFERENCES

(1) Li, K.; Sun, Y. Electrocatalytic Upgrading of Biomass-Derived Intermediate Compounds to Value-Added Products. *Chem.—Eur. J.* **2018**, *24*, 18258−18270.

(2) Kwon, Y.; Schouten, K. J. P.; van der Waal, J. C.; de Jong, E.; Koper, M. T. M. Electrocatalytic Conversion of Furanic Compounds. *ACS Catal.* **2016**, *6*, 6704−6717.

(3) Du, L.; Shao, Y.; Sun, J.; Yin, G.; Du, C.; Wang, Y. Electrocatalytic Valorisation of Biomass Derived Chemicals. *Catal. Sci. Technol.* **2018**, *8*, 3216−3232.

(4) Möhle, S.; Zirbes, M.; Rodrigo, E.; Gieshoff, T.; Wiebe, A.; Waldvogel, S. R. Modern Electrochemical Aspects for the Synthesis of Value-Added Organic Products. *Angew. Chem., Int. Ed.* **2018**, *57*, 6018−6041.

(5) Mettler, M. S.; Vlachos, D. G.; Dauenhauer, P. J. Top Ten Fundamental Challenges of Biomass Pyrolysis for Biofuels. *Energy Environ. Sci.* **2012**, *5*, 7797−7813.

(6) Chadderdon, X. H.; Chadderdon, D. J.; Matthiesen, J. E.; Qiu, Y.; Carraher, J. M.; Tessonnier, J.-P.; Li, W. Mechanisms of Furfural Reduction on Metal Electrodes: Distinguishing Pathways for Selective Hydrogenation of Bioderived Oxygenates. *J. Am. Chem. Soc.* **2017**, *139*, 14120−14128.

(7) Shan, N.; Hanchett, M. K.; Liu, B. Mechanistic Insights Evaluating Ag, Pb, and Ni as Electrocatalysts for Furfural Reduction from First-Principles Methods. *J. Phys. Chem. C* **2017**, *121*, 25768−25777.

(8) Zhao, B.; Chen, M.; Guo, Q.; Fu, Y. Electrocatalytic Hydrogenation of Furfural to Furfuryl Alcohol using Platinum Supported on Activated Carbon Fibers. *Electrochim. Acta* **2014**, *135*, 139−146.

(9) Jung, S.; Biddinger, E. J. Controlling Competitive Side Reactions in the Electrochemical Upgrading of Furfural to Biofuel. *Energy Technol.* **2018**, *6*, 1370−1379.

(10) Gupta, K.; Rai, R. K.; Singh, S. K. Metal Catalysts for the Efficient Transformation of Biomass-derived HMF and Furfural to Value Added Chemicals. *ChemCatChem* **2018**, *10*, 2326−2349.

(11) Douthwaite, M.; Huang, X.; Iqbal, S.; Miedziak, P. J.; Brett, G. L.; Kondrat, S. A.; Edwards, J. K.; Sankar, M.; Knight, D. W.; Bethell, D. The Controlled Catalytic Oxidation of Furfural to Furoic Acid Using AuPd/$Mg(OH)_2$. *Catal. Sci. Technol.* **2017**, *7*, 5284−5293.

(12) Soták, T.; Hronec, M.; Gál, M.; Dobročka, E.; Škriniarová, J. Aqueous-Phase Oxidation of Furfural to Maleic Acid Catalyzed by Copper Phosphate Catalysts. *Catal. Lett.* **2017**, *147*, 2714−2723.

(13) Shi, S.; Guo, H.; Yin, G. Synthesis of Maleic Acid from Renewable Resources: Catalytic Oxidation of Furfural in Liquid Media with Dioxygen. *Catal. Commun.* **2011**, *12*, 731−733.

(14) Araji, N.; Madjinza, D. D.; Chatel, G.; Moores, A.; Jérôme, F.; De Oliveira Vigier, K. Synthesis of Maleic and Fumaric Acids from Furfural in the Presence of Betaine Hydrochloride and Hydrogen Peroxide. *Green Chem.* **2017**, *19*, 98−101.

(15) Alonso-Fagúndez, N.; Agirrezabal-Telleria, I.; Arias, P. L.; Fierro, J. L. G.; Mariscal, R.; Granados, M. L. Aqueous-phase Catalytic Oxidation of Furfural with H_2O_2: High Yield of Maleic Acid by using Titanium Silicalite-1. *RSC Adv.* **2014**, *4*, 54960−54972.

(16) Alonso-Fagúndez, N.; Ojeda, M.; Mariscal, R.; Fierro, J. L. G.; López Granados, M. Gas Phase Oxidation of Furfural to Maleic Anhydride on V_2O_5/γ-Al_2O_3 Catalysts: Reaction Conditions to Slow Down the Deactivation. *J. Catal.* **2017**, *348*, 265−275.

(17) Li, X.; Ko, J.; Zhang, Y. Highly Efficient Gas-Phase Oxidation of Renewable Furfural to Maleic Anhydride over Plate Vanadium Phosphorus Oxide Catalyst. *ChemSusChem* **2018**, *11*, 612−618.

(18) Li, X.; Wan, W.; Kattel, S.; Chen, J. G.; Wang, T. Selective Hydrogenation of Biomass-derived 2(5H)-Furanone over Pt-Ni and Pt-Co Bimetallic Catalysts: From Model Surfaces to Supported Catalysts. *J. Catal.* **2016**, *344*, 148−156.

(19) Mariscal, R.; Maireles-Torres, P.; Ojeda, M.; Sádaba, I.; López Granados, M. Furfural: A Renewable and Versatile Platform Molecule for the Synthesis of Chemicals and Fuels. *Energy Environ. Sci.* **2016**, *9*, 1144−1189.

(20) Chen, B.; Li, F.; Yuan, G. Selective Hydrodeoxygenation of 5-Hydroxy-2(5H)-furanone to γ-Butyrolactone over Pt/Mesoporous Solid Acid Bifunctional Catalyst. *RSC Adv.* **2017**, *7*, 21145−21152.

(21) Alba-Rubio, A. C.; Fierro, J. L. G.; León-Reina, L.; Mariscal, R.; Dumesic, J. A.; López Granados, M. Oxidation of Furfural in Aqueous H_2O_2 Catalysed by Titanium Silicalite: Deactivation Processes and Role of Extraframework Ti Oxides. *Appl. Catal., B* **2017**, *202*, 269−280.

(22) Shen, G.; Zhang, S.; Lei, Y.; Chen, Z.; Yin, G. Synthesis of 2,5-Furandicarboxylic Acid by Catalytic Carbonylation of Renewable Furfural Derived 5-Bromofuroic Acid. *Mol. Catal.* **2018**, *455*, 204−209.

(23) Dick, G. R.; Frankhouser, A. D.; Banerjee, A.; Kanan, M. W. A Scalable Carboxylation Route to Furan-2,5-dicarboxylic Acid. *Green Chem.* **2017**, *19*, 2966−2972.

(24) Payne, K. A. P.; Marshall, S. A.; Fisher, K.; Cliff, M. J.; Cannas, D. M.; Yan, C.; Heyes, D. J.; Parker, D. A.; Larrosa, I.; Leys, D. Enzymatic Carboxylation of 2-Furoic Acid Yields 2,5-Furandicarboxylic Acid (FDCA). *ACS Catal.* **2019**, *9*, 2854−2865.

(25) Li, X.; Jia, P.; Wang, T. Furfural: A Promising Platform Compound for Sustainable Production of C4 and C5 Chemicals. *ACS Catal.* **2016**, *6*, 7621−7640.

(26) Nilges, P.; Schröder, U. Electrochemistry for Biofuel Generation: Production of Furans by Electrocatalytic Hydrogenation of Furfurals. *Energy Environ. Sci.* **2013**, *6*, 2925.
(27) Gilkey, M. J.; Xu, B. Heterogeneous Catalytic Transfer Hydrogenation as an Effective Pathway in Biomass Upgrading. *ACS Catal.* **2016**, *6*, 1420−1436.
(28) Knez, Ž.; Markočič, E.; Hrnčič, M. K.; Ravber, M.; Škerget, M. High Pressure Water Reforming of Biomass for Energy and Chemicals: A Short Review. *J. Supercrit. Fluids* **2015**, *96*, 46−52.
(29) Byun, J.; Ahn, Y.; Kim, J.; Kim, J.-R.; Jeong, S.-Y.; Kim, B.-S.; Kim, H. J.; Han, J. Integrated Process for Electrocatalytic Conversion of Glycerol to Chemicals and Catalytic Conversion of Corn Stover to Fuels. *Energy Convers. Manage.* **2018**, *163*, 180−186.
(30) Green, S. K.; Lee, J.; Kim, H. J.; Tompsett, G. A.; Kim, W. B.; Huber, G. W. The Electrocatalytic Hydrogenation of Furanic Compounds in a Continuous Electrocatalytic Membrane Reactor. *Green Chem.* **2013**, *15*, 1869.
(31) Kubota, S. R.; Choi, K. S. Electrochemical Oxidation of 5-Hydroxymethylfurfural to 2,5-Furandicarboxylic Acid (FDCA) in Acidic Media Enabling Spontaneous FDCA Separation. *ChemSusChem* **2018**, *11*, 2138−2145.
(32) Cha, H. G.; Choi, K.-S. Combined Biomass Valorization and Hydrogen Production in a Photoelectrochemical Cell. *Nat. Chem.* **2015**, *7*, 328−333.
(33) Nam, D.-H.; Taitt, B. J.; Choi, K.-S. Copper-Based Catalytic Anodes To Produce 2,5-Furandicarboxylic Acid, a Biomass-Derived Alternative to Terephthalic Acid. *ACS Catal.* **2018**, *8*, 1197−1206.
(34) Lv, G.; Chen, S.; Zhu, H.; Li, M.; Yang, Y. Determination of the Crucial Functional Groups in Graphene Oxide for Vanadium Oxide Nanosheet Fabrication and its Catalytic Application in 5-Hydroxymethylfurfural and Furfural Oxidation. *J. Cleaner Prod.* **2018**, *196*, 32−41.
(35) Roylance, J. J.; Kim, T. W.; Choi, K.-S. Efficient and Selective Electrochemical and Photoelectrochemical Reduction of 5-Hydroxymethylfurfural to 2,5-Bis(hydroxymethyl)furan Using Water as the Hydrogen Source. *ACS Catal.* **2016**, *6*, 1840−1847.
(36) You, B.; Liu, X.; Jiang, N.; Sun, Y. A General Strategy for Decoupled Hydrogen Production from Water Splitting by Integrating Oxidative Biomass Valorization. *J. Am. Chem. Soc.* **2016**, *138*, 13639−13646.
(37) Vuyyuru, K. R.; Strasser, P. Oxidation of Biomass Derived 5-Hydroxymethylfurfural using Heterogeneous and Electrochemical Catalysis. *Catal. Today* **2012**, *195*, 144−154.
(38) Chadderdon, D. J.; Xin, L.; Qi, J.; Qiu, Y.; Krishna, P.; More, K. L.; Li, W. Electrocatalytic Oxidation of 5-Hydroxymethylfurfural to 2,5-Furandicarboxylic Acid on Supported Au and Pd Bimetallic Nanoparticles. *Green Chem.* **2014**, *16*, 3778−3786.
(39) Kubota, S. R.; Choi, K.-S. Electrochemical Valorization of Furfural to Maleic Acid. *ACS Sustainable Chem. Eng.* **2018**, *6*, 9596−9600.
(40) Parpot, P.; Bettencourt, A. P.; Chamoulaud, G.; Kokoh, K. B.; Belgsir, E. M. Electrochemical investigations of the oxidation-reduction of furfural in aqueous medium. *Electrochim. Acta* **2004**, *49*, 397−403.
(41) Chamoulaud, G.; Floner, D.; Moinet, C.; Lamy, C.; Belgsir, E. M. Biomass Conversion II: Simultaneous Electrosyntheses of Furoic Acid and Furfuryl Alcohol on Modified Graphite Felt Electrodes. *Electrochim. Acta* **2001**, *46*, 2757−2760.
(42) Jiang, N.; Liu, X.; Dong, J.; You, B.; Liu, X.; Sun, Y. Electrocatalysis of Furfural Oxidation Coupled with H_2 Evolution via Nickel-Based Electrocatalysts in Water. *ChemNanoMat* **2017**, *3*, 491−495.
(43) Gong, L.; Agrawal, N.; Roman, A.; Holewinski, A.; Janik, M. J. Density functional theory study of furfural electrochemical oxidation on the Pt (1 1 1) surface. *J. Catal.* **2019**, *373*, 322−335.
(44) Pourbaix, M. *Atlas of Electrochemical Equilibria in Aqueous Solutions*, 2nd ed.; Franklin, J. A., Ed.; Translator; National Association of Corrosion Engineers: Houston, TX, 1974; pp 378−383.
(45) Kwon, Y.; Schouten, K. J. P.; Koper, M. T. M. Mechanism of the Catalytic Oxidation of Glycerol on Polycrystalline Gold and Platinum Electrodes. *ChemCatChem* **2011**, *3*, 1176−1185.
(46) Cuesta, A.; Cabello, G.; Osawa, M.; Gutiérrez, C. Mechanism of the Electrocatalytic Oxidation of Formic Acid on Metals. *ACS Catal.* **2012**, *2*, 728−738.
(47) Verdeguer, P.; Merat, N.; Gaset, A. Lead/Platinum on Charcoal as Catalyst for Oxidation of Furfural. Effect of Main Parameters. *Appl. Catal., A* **1994**, *112*, 1−11.
(48) Osawa, M. Dynamic Processes in Electrochemical Reactions Studied by Surface-Enhanced Infrared Absorption Spectroscopy (SEIRAS). *Bull. Chem. Soc. Jpn.* **1997**, *70*, 2861−2880.
(49) Ye, S.; Inchihara, T.; Uosaki, K. Spectroscopic Studies on Electroless Deposition of Copper on a Hydrogen-Terminated Si(111) Surface in Fluoride Solutions. *J. Electrochem. Soc.* **2001**, *148*, C421.
(50) Miki, A.; Ye, S.; Osawa, M. Surface-Enhanced IR Absorption on Platinum Nanoparticles: An Application to Real-time Monitoring of Electrocatalytic Reactions. *Chem. Commun.* **2002**, *14*, 1500−1501.
(51) Kwon, Y.; Schouten, K. J. P.; Koper, M. T. M. Mechanism of the Catalytic Oxidation of Glycerol on Polycrystalline Gold and Platinum Electrodes. *ChemCatChem* **2011**, *3*, 1176−1185.
(52) Hansen, H. A.; Rossmeisl, J.; Nørskov, J. K. Surface Pourbaix Diagrams and Oxygen Reduction Activity of Pt, Ag and Ni(111) Surfaces Studied by DFT. *Phys. Chem. Chem. Phys.* **2008**, *10*, 3722−3730.
(53) Jerkiewicz, G.; Vatankhah, G.; Lessard, J.; Soriaga, M.; Park, Y. Surface-Oxide Growth at Platinum Electrodes in Aqueous H_2SO_4. *Electrochim. Acta* **2004**, *49*, 1451−1459.
(54) Clauson-Kass, N.; Fakstorp, J. Nuclear Oxidation of Furfural. *Acta Chem. Scand.* **1947**, *1*, 415−421.
(55) Dunlop, A. P.; Stout, P. R.; Swadesh, S. Autoxidation of Furfural. *Ind. Eng. Chem.* **1946**, *38*, 705−708.
(56) Planes, G. A.; Moran, E.; Rodriguez, J. L.; Barbero, C.; Pastor, E. Electrochemical Behavior of Benzaldehyde on Polycrystalline Platinum. An in Situ FTIR and DEMS Study. *Langmuir* **2003**, *19*, 8899−8906.
(57) Gui, J. Y.; Stern, D. A.; Lu, F.; Hubbard, A. T. Surface chemistry of five-membered heteroaromatics at Pt(III) electrodes studied by EELS, LEED, Auger spectroscopy and electrochemistry: furan, pyrrole and thiophene. *J. Electroanal. Chem.* **1991**, *305*, 37−55.
(58) Hallal, J. L. J.; Lucho, A. M. S.; Gonçalves, R. S. Electrochemical Polymerization of Furfural on a Platinum Electrode in Aqueous Solutions of Potassium Biphthalate. *Mater. Res.* **2005**, *8*, 23−29.
(59) Serpa Lucho, A. M.; Joaquim Hallal, J. L.; Simões Gonçalves, R. Evidence of a Polymeric Film Formation from Furfural Electrooxidation on Platinum Platinized Electrode in Acetonitrile. *J. Macromol. Sci., Pure Appl. Chem.* **2003**, *40*, 933−946.
(60) Holewinski, A.; Linic, S. Elementary Mechanisms in Electrocatalysis: Revisiting the ORR Tafel Slope. *J. Electrochem. Soc.* **2012**, *159*, H864−H870.
(61) Román, A. M.; Dudoff, J.; Baz, A.; Holewinski, A. Identifying "Optimal" Electrocatalysts: Impact of Operating Potential and Charge Transfer Model. *ACS Catal.* **2017**, *7*, 8641−8652.
(62) Schnaidt, J.; Heinen, M.; Denot, D.; Jusys, Z.; Jürgen Behm, R. Electrooxidation of Glycerol Studied by Combined In Situ IR Spectroscopy and Online Mass Spectrometry under Continuous Flow Conditions. *J. Electroanal. Chem.* **2011**, *661*, 250−264.
(63) Williams, R. M.; Pang, S. H.; Medlin, J. W. Ring-Opening and Oxidation Pathways of Furanic Oxygenates on Oxygen-Precovered Pd(111). *J. Phys. Chem. C* **2014**, *118*, 27933−27943.
(64) Shi, D.; Vohs, J. M. Deoxygenation of Biomass-Derived Oxygenates: Reaction of Furfural on Zn-Modified Pt(111). *ACS Catal.* **2015**, *5*, 2177−2183.
(65) Taylor, M. J.; Jiang, L.; Reichert, J.; Papageorgiou, A. C.; Beaumont, S. K.; Wilson, K.; Lee, A. F.; Barth, J. V.; Kyriakou, G. Catalytic Hydrogenation and Hydrodeoxygenation of Furfural over Pt(111): A Model System for the Rational Design and Operation of

DOI: 10.1021/acscatal.9b02656
ACS Catal. 2019, 9, 10305−10316

Practical Biomass Conversion Catalysts. *J. Phys. Chem. C* **2017**, *121*, 8490−8497.
(66) Mark, L. O.; Jenkins, A. H.; Heinz, H.; Medlin, J. W. Furfuryl Alcohol Deoxygenation, Decarbonylation, and Ring-Opening on Pt(111). *Surf. Sci.* **2018**, *677*, 333−340.
(67) Han, B.; Li, Z.; Wandlowski, T. Adsorption and Self-Assembly of Aromatic Carboxylic Acids on Au/Electrolyte Interfaces. *Anal. Bioanal. Chem.* **2007**, *388*, 121−129.
(68) Montilla, F.; Morallón, E.; Vázquez, J. L. Electrochemical Behaviour of Benzoic Acid on Platinum and Gold Electrodes. *Langmuir* **2003**, *19*, 10241−10246.
(69) Abd-El-Latif, A. A.; Bondue, C. J.; Ernst, S.; Hegemann, M.; Kaul, J. K.; Khodayari, M.; Mostafa, E.; Stefanova, A.; Baltruschat, H. Insights into Electrochemical Reactions by Differential Electrochemical Mass Spectrometry. *Trends Anal. Chem.* **2015**, *70*, 4−13.
(70) Zhou, Y.; Shen, Y.; Piao, J. Sustainable Conversion of Glycerol into Value-Added Chemicals by Selective Electro-Oxidation on Pt-Based Catalysts. *ChemElectroChem* **2018**, *5*, 1624.
(71) Kim, H. J.; Lee, J.; Green, S. K.; Huber, G. W.; Kim, W. B. Selective Glycerol Oxidation by Electrocatalytic Dehydrogenation. *ChemSusChem* **2014**, *7*, 1051−1056.
(72) Kim, S.; Evans, T. J.; Mukarakate, C.; Bu, L.; Beckham, G. T.; Nimlos, M. R.; Paton, R. S.; Robichaud, D. J. Furan Production from Glycoaldehyde over HZSM-5. *ACS Sustainable Chem. Eng.* **2016**, *4*, 2615−2623.
(73) Kul'nevich, V. G.; Badovskaya, L. A.; Muzychenko, G. F. 2-Formyloxyfuran as an Intermediate in the Hydrogen Peroxide Oxidation of Furfuraldehyde. *Chem. Heterocycl. Compd.* **1970**, *6*, 535−537.
(74) Petersen, J. B.; Lei, J.; Clauson-Kaas, N.; Norris, K. *The Chemistry of Endialone*, Mathematical-Physical Letters; Munksgaard, 1967; Vol. *36*, pp 1−23.
(75) Greuter, H.; Winkler, T. Die Struktur der durch Halogenierung von Furfural in Wasser gebildeten Oxydationsprodukte. *Helv. Chim. Acta* **1978**, *61*, 3103−3107.
(76) Muzychenko, G. F.; Badovskaya, L. A.; Kul'nevich, V. G. Role of Water in the Oxidation of Furfural with Hydrogen Peroxide. *Chem. Heterocycl. Compd.* **1972**, *8*, 1311−1313.
(77) Blasini, D. R.; Rochefort, D.; Fachini, E.; Alden, L. R.; DiSalvo, F. J.; Cabrera, C. R.; Abruña, H. D. Surface Composition of Ordered Intermetallic Compounds PtBi and PtPb. *Surf. Sci.* **2006**, *600*, 2670−2680.
(78) Lovic, J.; Tripkovic, D.; Popovic, K.; Jovanovic, V.; Tripkovic, A. Electrocatalytic properties of Pt-Bi electrodes towards the electrooxidation of formic acid. *J. Serb. Chem. Soc.* **2013**, *78*, 1189−1202.
(79) Schoenbaum, C. A.; Schwartz, D. K.; Medlin, J. W. Controlling the Surface Environment of Heterogeneous Catalysts Using Self-Assembled Monolayers. *Acc. Chem. Res.* **2014**, *47*, 1438−1445.
(80) Pang, S. H.; Román, A. M.; Medlin, J. W. Adsorption Orientation-Induced Selectivity Control of Reactions of Benzyl Alcohol on Pd(111). *J. Phys. Chem. C* **2012**, *116*, 13654−13660.
(81) Zhang, S.; Lan, J.; Chen, Z.; Yin, G.; Li, G. Catalytic Synthesis of 2,5-Furandicarboxylic Acid from Furoic Acid: Transformation from C5 Platform to C6 Derivatives in Biomass Utilizations. *ACS Sustainable Chem. Eng.* **2017**, *5*, 9360−9369.
(82) Kim, H. J.; Choi, S. M.; Seo, M. H.; Green, S.; Huber, G. W.; Kim, W. B. Efficient Electrooxidation of Biomass-Derived Glycerol over a Graphene-Supported PtRu Electrocatalyst. *Electrochem. Commun.* **2011**, *13*, 890−893.
(83) Koper, M. T. M. Electrocatalysis on Bimetallic and Alloy Surfaces. *Surf. Sci.* **2004**, *548*, 1−3.

DOI: 10.1021/acscatal.9b02656
ACS Catal. 2019, 9, 10305−10316